International Journal of
Environmental Research and Public Health

MDPI

Article

Pristine and Magnetic Kenaf Fiber Biochar for Cd^{2+} Adsorption from Aqueous Solution

Anwar Ameen Hezam Saeed [1,2], Noorfidza Yub Harun [1,2,*], Suriati Sufian [1], Muhammad Roil Bilad [3], Zaki Yamani Zakaria [4], Ahmad Hussaini Jagaba [5], Aiban Abdulhakim Saeed Ghaleb [5] and Haetham G. Mohammed [6]

1 Department of Chemical Engineering, University Teknologi PETRONAS, Seri Iskandar 31750, Malaysia; anwar_17006829@utp.edu.my (A.A.H.S.); suriati@utp.edu.my (S.S.)
2 Centre of Urban Resource Sustainability, University Teknologi PETRONAS, Bandar Seri Iskandar 32610, Malaysia
3 Faculty of Integrated Technologies, University Brunei Darussalam, Jalan Tungku Link, Gadong BE1410, Brunei; roil.bilad@ubd.edu.bn
4 School of Chemical & Energy Engineering, University Teknologi Malaysia, Skudai 81310, Malaysia; zakiyamani@utm.my
5 Department of Civil and Environmental Engineering, University Teknologi PETRONAS, Bandar Seri Iskandar 32610, Malaysia; ahjagaba@gmail.com (A.H.J.); aiban_17004546@utp.edu.my (A.A.S.G.)
6 Department of Mechanical Engineering, University Teknologi PETRONAS, Bandar Seri Iskandar 32610, Malaysia; haetham_19000233@utp.edu.my
* Correspondence: noorfidza.yub@utp.edu.my

Citation: Saeed, A.A.H.; Harun, N.Y.; Sufian, S.; Bilad, M.R.; Zakaria, Z.Y.; Jagaba, A.H.; Ghaleb, A.A.S.; Mohammed, H.G. Pristine and Magnetic Kenaf Fiber Biochar for Cd^{2+} Adsorption from Aqueous Solution. *Int. J. Environ. Res. Public Health* **2021**, *18*, 7949. https://doi.org/10.3390/ijerph18157949

Academic Editor: Yuping Qiu

Received: 2 June 2021
Accepted: 20 July 2021
Published: 27 July 2021

Abstract: Development of strategies for removing heavy metals from aquatic environments is in high demand. Cadmium is one of the most dangerous metals in the environment, even under extremely low quantities. In this study, kenaf and magnetic biochar composite were prepared for the adsorption of Cd^{2+}. The synthesized biochar was characterized using (a vibrating-sample magnetometer VSM), Scanning electron microscopy (SEM), X-ray powder diffraction (XRD), Fourier-transform infrared spectroscopy (FTIR), and X-ray photoelectron spectroscopy (XPS). The adsorption batch study was carried out to investigate the influence of pH, kinetics, isotherm, and thermodynamics on Cd^{2+} adsorption. The characterization results demonstrated that the biochar contained iron particles that help in improving the textural properties (i.e., surface area and pore volume), increasing the number of oxygen-containing groups, and forming inner-sphere complexes with oxygen-containing groups. The adsorption study results show that optimum adsorption was achieved under pH 5–6. An increase in initial ion concentration and solution temperature resulted in increased adsorption capacity. Surface modification of biochar using iron oxide for imposing magnetic property allowed for easy separation by external magnet and regeneration. The magnetic biochar composite also showed a higher affinity to Cd^{2+} than the pristine biochar. The adsorption data fit well with the pseudo-second-order and the Langmuir isotherm, with the maximum adsorption capacity of 47.90 mg/g.

Keywords: adsorption; heavy metals; magnetic biochar; iron oxides; kenaf fiber; synthesis; aqueous solution; cadmium

1. Introduction

Water resources have been harmed by a variety of toxins, including heavy metals, dyes, surfactants, phenols, and other personal care chemicals [1–3]. Since heavy metal waste almost does not dissolve into harmless materials, it accumulates and is toxic to humans. It is also currently amongst the most important environmental concerns. Cadmium is one of the most harmful heavy metals, having been identified as a human carcinogen and teratogen with effects on the lungs, liver, and kidney [4–6].

Cadmium is naturally found in the environment as a result of the gradual erosion and abrasion of rocks and soils, as well as one-time events such as forest fires and volcanic

eruptions [7–9]. As a result, it can be found naturally in the air, water, and soils. Cadmium is also unnaturally extracted from paint pigment, paints, garment manufacturing, battery manufacturing, gasoline manufacturing, and fertilizer manufacturing industries [10,11]. The permissible concentration of cadmium in drinking water has been set very low by the United States Environmental Protection Agency (the US EPA) at 0.005 mg/L, and even lower, at 0.003 mg/L, by the World Health Organization. Therefore, cadmium must be removed from wastewater before it can be discharged into environmental sources and contaminate the water resources [12–14].

Membrane-based separation, electrochemical deposition, chemical precipitation, coagulation, solvent extraction, ion exchange, and adsorption have all been explored to reduce the concentration of cadmium to an acceptable level and meet the environmental requirement [15]. Although all the aforementioned technologies are highly effective in removing heavy metals, they have significant drawbacks such as byproduct formation, large sludge production, and high energy requirements [16]. Adsorption is considered an attractive method due to its simplicity, cost-effectiveness, and the possibility of using it on a large scale [17–19]. Many adsorbents' materials have been applied in industries, such as activated carbon, activated alumina, silica gel, molecular sieve carbon, molecular sieve zeolites, and polymeric adsorbents [3,20,21].

An ideal adsorbent material should have a large surface area, maximum adsorption power, mechanical stability, and the ability to be easily separated and regenerated [22]. Biochar has been considered as the promising adsorbent material due to its excellent adsorption capacities for heavy metals and organic pollutants in an aqueous solution [23,24]. Biochar is a solid product of biomass pyrolysis where pyrolysis occurs in the absence of oxygen at the high-temperature heating process for biofuel production [25,26]. Essentially, biochar production aims to produce energy or reduce the amount of biomass feedstock used. However, there has been a lot of emphasis on improving the pyrolysis conditions to increase yield and biochar properties [27–29].

The spent biochar suspended in an aqueous medium usually requires centrifugation and filtration measures for recovery. Such recovery process limits the use of biochar in wastewater treatment on a large scale. Furthermore, during these measures, pollutants adsorbed on the biochar may desorb, resulting in secondary pollution [30–32]. As a result, it is critical to address biochar's flaws to increase its effectiveness in water contamination mitigation. Studies from the literature have proven that biochar can remove toxic compounds, but pristine biochar has a limited ability to adsorb heavy metals from wastewater [33]. Several types of feedstocks have been used and treated as biochar-based adsorbents for cadmium removal, such as alamo switchgrass [34], pine wood residues [35], pig manure [36], rice husk [29,37], dairy manure, oak wood [38], pine bark [38], and corn stalk [39].

Surface modification is a proper method to improve biochar properties. Biochar is typically rich in functional groups such as hydroxyl, carboxyl, carbonyl, and methylene on the surfaces of the pore system [40]. Biochar has a large surface area and strong adsorption efficiency that makes it attractive for the removal of heavy metals from wastewater [41]. Surface modification is categorized into activation and formation of composite [42]. Activation is usually carried out by physical or chemical activation, both of which are conventional and have been known about for a long time [43,44]. The biochar-based composite as part of biochar surface modification is usually carried out by modifying the biochar with other materials such as clay, carbonaceous materials, microorganism, organic compound, and metal oxide [45]. Those composites adjust the properties of biochar and improve their functional groups. Biochar surface modification technology is better than primary chemical and physical activation, where the surface modification creates new functional groups that are not present in either biochar or raw materials [42,46].

Biochar-based composite is still in its infancy. It is mainly used in industries, especially those targeting to adsorb specific pollutants where the biochar is specially synthesized to have a specific affinity to the limited pollutants [47]. Biochar has a negative surface charge with high surface area and large pore volume [48]. Those features allow biochar to be a

sufficient and promising adsorbent due to distinct adsorption on oxygenated functional groups, electrostatic attraction to aromatic groups, and precipitation on the mineral of biochar [49–51]. The biochar-based metal oxide can extract negatively charged oxyanion from an aqueous solution by using the high surface area of biochar as a medium to embed metal oxide with contacting chemical properties [52–54].

Recently, biochar surface modification using metal oxide has been employed. Agrafioti et al. [55] used this technology and found out that soaking raw materials (rice husk) and biochar derived from municipal waste with iron powder $FeCl_3$ before pyrolysis created a positive charge which helped to adsorb arsenic from aqueous solution. Vladimir et al. [56] used corncob biochar composite with $FeCl_3$ and found a similar result to Agrafioti, in which the product efficiently adsorbed arsenic. Attempts have been made to use iron's magnetic properties to produce magnetic biochar that can remove contaminants in pinewood biomass by compositing biochar with hematite, as reported by Wang et al. [57], which resulted in the double performance of sorption capacity in comparison with the pristine biochar. Akila et al. [58] and Khan et al. [59] used magnetic biochar to adsorb lead and cadmium from an aqueous solution and discovered that it was effective and easily separated.

In this study, magnetic biochar has been synthesized and developed from kenaf biochar and Fe_3O_4. The pristine and magnetic biochar were characterized by a vibrating-sample magnetometer (VSM), scanning electron microscope (SEM) X-ray diffraction (XRD), Fourier transform infrared spectroscopy (FTIR), and X-ray photoelectron spectroscopy (XPS). Adsorption isotherm, kinetics, and thermodynamic of Cd^{2+} with this magnetic biochar-based adsorbent have been investigated. Consecutively the effect of pH, initial concentration, and time on the adsorption process was also studied.

2. Materials and Methods

2.1. Materials

The kenaf fiber was collected from a kenaf plantation in Pahang, Malaysia. After collection, it was washed, sieved, and prepared for biochar production. Other chemicals, such as sodium hydroxide, sodium nitrate, hydrochloric acid, cadmium nitrate trihydrate, ferrous and ferric chloride, and ethanol, were purchased from (Sigma-Aldrich (M) Sdn Bhd, Selangor D.E, Malaysia). The chemicals were used as received without any treatment.

2.2. Methods

The preparation procedure of the composite magnetic biochar-based adsorbent was divided into two stages: biochar production and modification, followed by adsorption testing (Figure 1). In biochar production, the raw kenaf was first pyrolyzed with different input parameters such as pyrolysis temperature, heating time, and impregnation ratio (raw kenaf/NaOH). The resulting biochars were then modified with magnet materials to produce composite magnetic biochar. The biochar and magnetic biochar were characterized then applied further for the Cd^{2+} adsorption process.

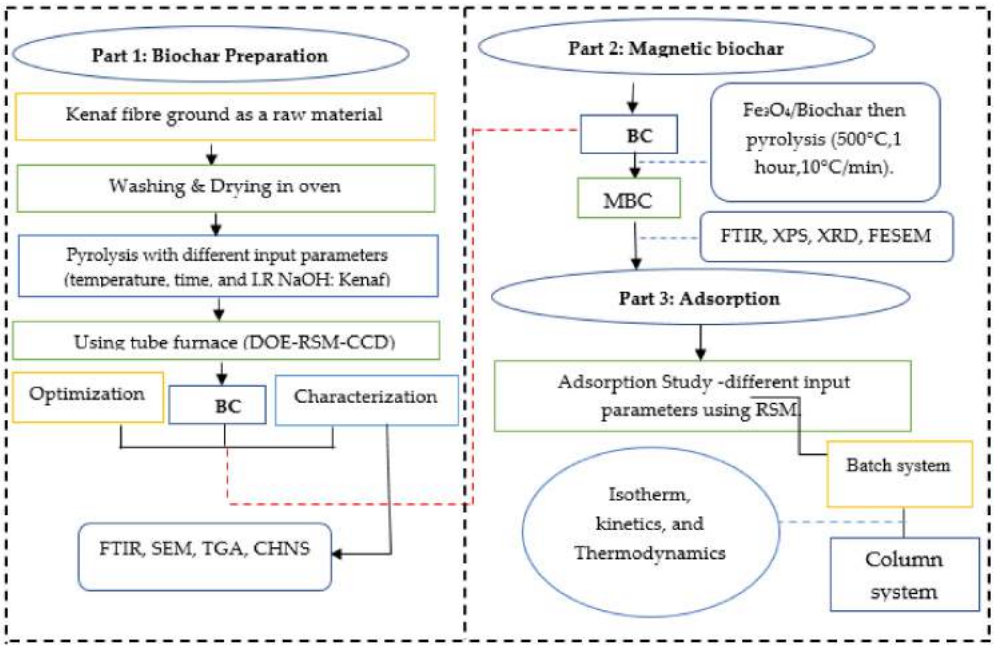

Figure 1. Summary chart of the composite magnetic biochar-based adsorbent preparation and testing. BC: biochar; MBC: magnetic biochar.

2.2.1. Biochar Preparation

The raw kenaf fiber was washed continuously with distilled water to remove the impurities and dust from its surface, followed by drying in an oven at 105 °C for 24 h. The dried sample was crushed to the desired mesh size of 0.5 mm by passing through the respective sieves (Vibratory Sieve Shaker AS 200 Digit cA Model). It was then stored in an airtight container at room temperature before use. Kenaf biochar was prepared by slow pyrolysis. The preparation parameters were preoptimized at pyrolysis temperature of 550 °C, 180 min reaction time, and 1:1 impregnation ratio with sodium hydroxide using tube furnace shown in in Figure 2 [60].

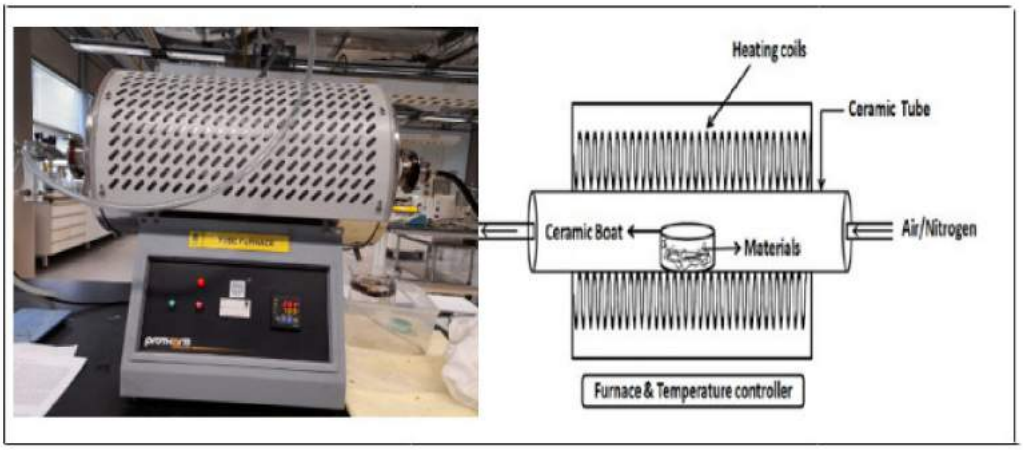

Figure 2. Schematic diagram of the tube furnace.

2.2.2. Magnetic Biochar Preparation

Magnetic biochar was synthesized by incorporating Fe_3O_4 nanoparticles. It was precipitated using methods employing ferric chloride ($FeCl_3.6H_2O$) and ferrous chloride ($FeCl_2.4H_2O$) with a ratio of 2:1, according to a protocol summarized in Figure 3 [61,62]. Subsequently, the prepared Fe_3O_4 was mixed with kenaf biochar and added into 150 mL

deionized water before being agitated for 45 min. This composite was sonicated and evaporated to dryness in a water bath for three hours at a constant temperature (100 °C).

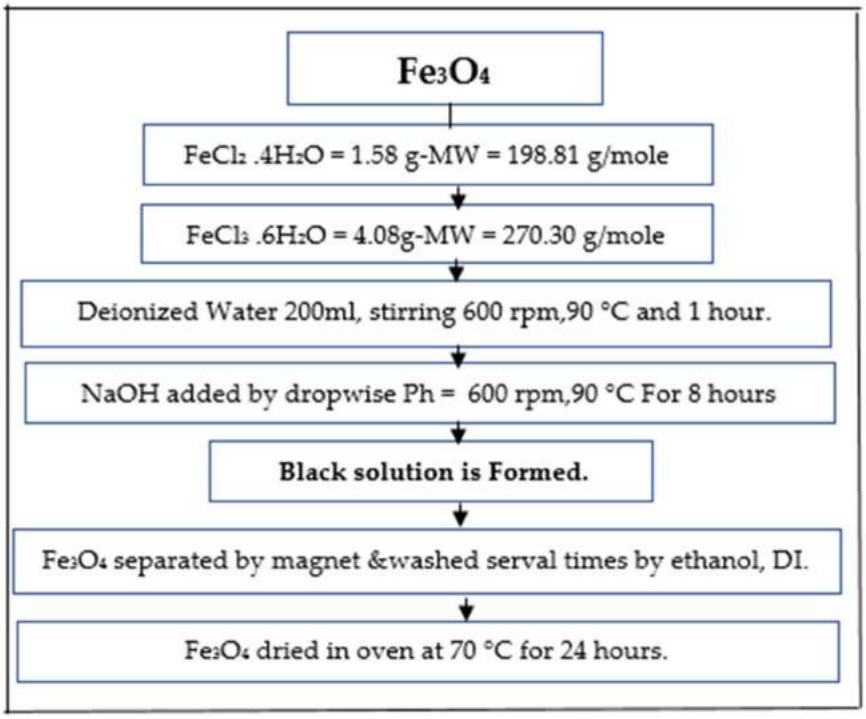

Figure 3. The synthesis procedure of Fe_3O_4 nanoparticles.

The composite magnetic biochar was subjected again to calcination at 500 °C in N_2 flow (600 cm^3/min) for 1 h at a 10 °C /min heating rate. After being cooled down to room temperature, the composite magnetic biochar was then washed again with distilled water to neutralize the pH.

2.3. Characterizations

The moisture content, volatile matter, ash content, and fixed carbon content were determined proximally using ASTM D7582-10 techniques. The contents of carbon (C), nitrogen (N), hydrogen (H), sulfur (S), oxygen (O), H/C, and O/C were detected using the Vario Micro Element Analyzer. The kenaf fiber biochar samples were cleaned and dried before being analyzed. The biochar samples were placed in the oven at 105 °C for 3 h for the measurement of moisture content. The volatile matter was determined by placing a closed crucible containing 2 g of biochar samples in a carbonite furnace at 950 °C for 10 min. The ash content was determined by placing a crucible containing 2 g of biochar sample in the furnace at 850 °C for 1 h. All these amounts were assessed using the difference between the initial and final weights.

The functional group analysis of the biochar samples was determined using Fourier-transform infrared spectroscopy (FTIR; Operant LLC, Madison, WI, USA). The FTIR spectra were recorded in wavelengths ranging from 400 to 4000 cm^{-1}. The FTIR plots were investigated to comprehend the possibility of a functional group's change. Scanning electron microscopy (SEM) coupled with energy-dispersive X-ray spectroscopy (EDS) was used to visualize the microstructure of biochar-based adsorbent and the elemental surface composition of the biochar-based adsorbent samples. SEM images were accomplished to detect the morphology and structural changes of the adsorbents. X-ray photoelectron spectroscopy (XPS) was employed to determine the mechanism of adsorption of samples with XPS spectrometers (Thermo Fisher Scientific, Waltham, MA). The specific surface area and the pore size of biochar were assessed using a Micromeritics ASAP 2020 analyzer.

A vibrating-sample magnetometer was used to analyze the magnetic properties of the magnetic biochar and raw synthesized iron oxide.

The pH values of the biochar adsorbents at the point-of-zero charges (PZC; pH_{pzc}) were obtained using the solid addition method (Balistrieri and Murray, 1981) [63]. By adding 1M NaOH or 1M HCl to the starting pH value (pH_i) of 0.1 M NaCl, the pH was raised from 2 to 11; 50 mL of this solution was then applied to a series of flasks, and 0.1 g biochar was added to each flask. The flasks were immediately capped, and the suspensions were agitated at 200 rpm for 3 h before the supernatant's final pH value (pH_f) was measured. The difference between pH_i and pH_f (Ph = pH_i pH_f) was plotted against pHi, and the point where the curve intersected with pH_i was pH_{PZC}.

2.4. Adsorption Study

A 1000 mg/L Cd (II) stock solution was prepared by dissolving 2.744 g of cadmium nitrate tetrahydrate in deionized water. Then, the stock solution was diluted to different concentrations for batch studies. The solution was treated with different parameters to obtain the best adsorption performance. The batch adsorption studies were conducted using an Erlenmeyer flask by loading the biochar in a cadmium aqueous solution. The fixed parameters were the dose of the adsorbent, the pH of the adsorbent, and the stirring speed. Parameters such as contact time, solution pH, initial concentration, and temperature were varied.

The effect of pH on the adsorption was identified by adjusting the pH value from 2 to 8 by adding 0.1 M hydrochloric acid and 0.1 M sodium hydroxide to change it from acidic to alkaline conditions. The sample was filtered using syringe filters and Whatman filter paper and analyzed for absorbance using atomic absorption spectrometry (AAS, Hitachi Z-5000). The removal efficiency (η, %) and adsorption capacity of magnetic biochar were determined using Equations (1) and (2):

$$\eta = \frac{\left(C_i - C_f\right)}{C_i} \times 100\% \quad (1)$$

$$q_e = \frac{\left(C_i - C_f\right)V}{m} \quad (2)$$

where C_i and C_f are Cd^{2+} concentrations (mg/L) at the initial and final stage, q_e is the adsorption capacity in mg/g, m denotes the quantity of magnetic biochar (g), and V is the volume of cadmium solution (L).

2.5. Kinetics, Isotherm, and Thermodynamic Analysis

Three different temperatures of 25, 35, and 45 °C were selected for evaluating the thermodynamics of adsorption. Table 1 specifies linearized forms of several isotherms of the Temkin, the Freundlich, and the Langmuir models. For adsorption kinetic analysis, various initial concentrations (of 5, 10, 20, 40, 60, 80, and 100 mg L^{-1}) were selected for the pseudo-first-order and pseudo-second-order kinetic models, as provided in Table 1. The pseudo-first-order (PFO) and pseudo-second-order (PSO) kinetic models are the most common models used to understand the adsorption mechanism and potential rate-limiting steps. The two models' formulas are listed in Table 1.

Table 1. Equilibrium and linearized equations of isotherm and kinetic models.

Model	Equilibrium	Linearized	Ref.
Langmuir	$Q_e = \frac{q_m b C_e}{1+bC_e}$	$\frac{C_e}{q_e} = \frac{1}{q_m b} + \frac{C_e}{q_m}$	[64]
Freundlich	$Q_e = K_f C_e^n$	$\log q_e = Log\ K_F + \frac{1}{n} \log C_e$	[65]
Temkin	$q_e = \frac{RT}{b} \ln(K_T C_e)$	$Q_e = B\ Ln\ K_T + B\ Ln\ Ce$	[66]
Pseudo-first-order	$q_t = q_e\left(1 - e^{-k_1 t}\right)$	$\ln(q_e - q_t) = lnq_e - k_1 t$	[67]
Pseudo-second-order	$q_t = \frac{q_e^2 k_2 t}{(1+q_e k_2 t)}$	$q_t = q_e\left(1 - e^{-k_1 t}\right)$	[68]

The Temkin, the Freundlich, and the Langmuir constants are denoted by K_T, K_F, and K_L, with corresponding units of L/mg, mg/g, and L/mg. Parameter B denotes the Temkin constant (J/mol).

3. Results and Discussion

3.1. Biochar Characteristic

3.1.1. Ultimate and Physical Properties

Table 2 summarizes the chemical and physical properties of the prepared biochars. The carbon, hydrogen, nitrogen, ash, and oxygen content of raw kenaf were 39.2, 5.12, 0.35, 16.32, and 43.6%; biochar were 67.52, 1.27, 1.23, 10.80, and 19.18%; magnetic biochars were 58.32, 1.12, 1.06, 13.75, and 25.75%, respectively.

Table 2. Selected chemical and physical properties of biochar and magnetic biochar.

Adsorbent	C%	H%	N%	O*%	Fe%	ash	O/C	H/C	S_{BET} ($m^2\ g^{-1}$)	Pore Volume ($cm^3\ g^{-1}$)	Pore Width (nm)
Kenaf (Raw)	39.2	5.12	0.35	43.6	N/A	16.32	1.12	0.130	4.50	0.009819	2.07
Biochar (550 °C)	67.52	1.27	1.23	19.18	N/A	10.80	0.284	0.0188	117.70	0.063884	2.17098
Magnetic Biochar	58.32	1.12	1.06	25.75	8.34	13.75	0.442	0.019	175.55	0.102366	2.33242

* calculated by difference; S_{BET}: surface read calculated by Brunauer–Emmett–Teller (BET) analysis.

The iron content of magnetic biochar was 8.34%, indicating that the surface of magnetic biochar was highly loaded with iron. The carbon content rose from 39.2 to 67.52%, while the oxygen content declined from 43.6 to 19.177%, indicating that the experimental conditions of the pyrolysis temperature and activation steps were the only significant contributors to the improvement of the biochar properties. The O/C ratio indicates the polarity and abundance of the polar oxygen-containing surface functional groups in biochar. A higher O/C ratio indicates more polar functional groups, which actively take part in the adsorption of cadmium. On the other hand, the H/C ratio indicates an aromaticity and stability of the biochar [69]. The magnetic biochar had a lower carbon content of 58.32% and high iron content compared to the pristine biochar, indicating that the carbon was significantly blended with the iron.

The specific surface area of raw kenaf, biochar, and magnetic biochar were 4.50, 117.70, and 175.55 $m^2\ g^{-1}$, respectively. These results indicate that the impregnation of iron oxide with biochar influenced the pore opening activation and pore structure of the pristine biochar, as also reported earlier [60].

3.1.2. Magnetic Properties

The magnetism curve in Figure 4 indicates that the magnetic biochar had super-paramagnetic properties with a magnetism M value of 19.98 emu g^{-1} and a retentivity (Mr) value of 1.62 emu g^{-1}. When comparing the magnetic properties of iron oxide and magnetic biochar, the magnetism and retentivity values of Fe_3O_4 and magnetic biochar were 55.10 emu/g and 3.5438 emu g^{-1}, while the magnetism and retentivity values of the magnetic biochar were 19.98 emu g^{-1} and 1.62 emu g^{-1}. These findings prove that after

incorporating magnetic particles, the magnetic biochar gained sufficient magnetism for recovery after use.

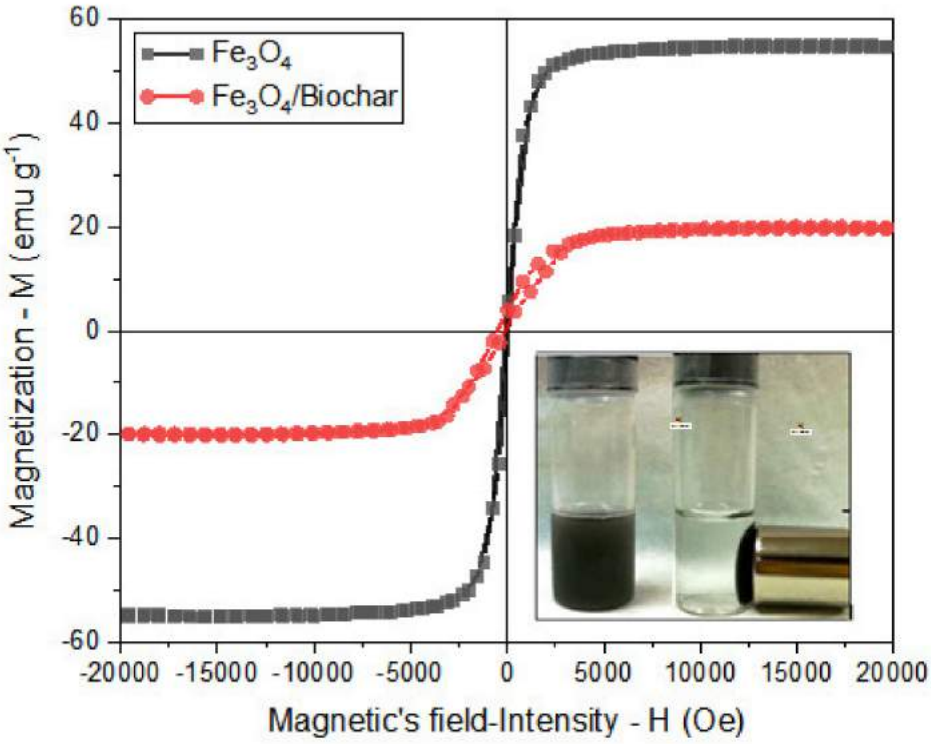

Figure 4. Magnetization curves of synthesized Fe_3O_4 nanoparticles and the magnetic biochar (Fe_3O_4/biochar). The inset shows the Fe_3O_4 nanoparticle under influence of a magnetic field.

3.1.3. Microstructure Analysis

Figure 5 illustrates the SEM images of raw kenaf, the biochar, and the magnetic biochar, as well as the magnetic biochar after adsorption. When compared to raw kenaf, the morphology of the biochar changed. The biochar SEM image in Figure 5b reveals micropores, macropores, and mesopores in several shapes. The biochar had a honeycomb-like morphology, with cylindrical holes intertwined with several big holes [70]. Many pore mouths in ordered manner can be seen over the surface of the biochar. The biochar was then subjected to magnetism and took on new shapes, indicating that surface modulation improved the textural properties and made it possible for Fe to adsorb onto the surface. The magnetic biochar SEM image (Figure 5a,d) shows particles trapped on the surface with plate-like roughness and distorted morphology containing sharp edges and corners, as seen in Figure 5c,d, as opposed to pristine biochar and raw kenaf, because the iron particles were filled in within the pristine biochar matrices which indicated good mechanical bounding [71].

3.1.4. XRD Analysis

Figure 6 shows the XRD analysis performed over the range of $2\theta = 10°–90°$ to classify the crystallographic structure changes of biochar, magnetic biochar, and the raw materials (kenaf and magnet). The XRD data (Figure 6d) shows that the magnetic biochar was amorphous, so the magnetite ores were loaded on the surfaces of the biochar. Amorphous biochar, which probably had a relatively homogeneous structure, could prevent the aggregation of the magnet nanoparticles and, therefore, maximize the adsorption capacity. According to Kang et al. [72], a good adsorption capacity is achieved by using amorphous adsorbent. Due to the thermochemical reactions between iron and carbon during pyrolysis, the amorphous carbon peak in the magnetic biochar pattern weakened greatly, resulting in a macrocrystalline graphite crystal lattice flaw. The magnetic biochar pattern's charac-

teristics peaks at 42.5°, 50.4°, 53.7°, and 57.8° show the presence of Fe in the biochar. The Fe_3O_4 phase was strongly crystalline and deposited on the composite's surface, as shown by the sharpness of the XRD peaks, and these findings are in agreement with studies done by Hongwei et al. [73] and Tassya et al. [74].

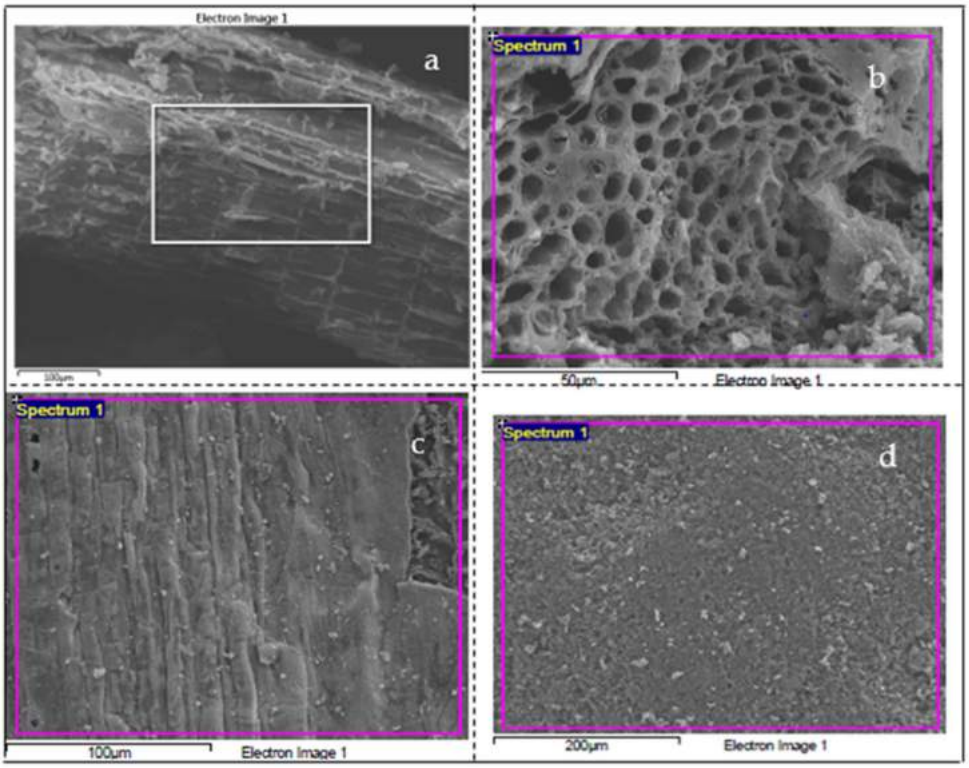

Figure 5. Scanning electron microscopy (SEM) images of (**a**) raw kenaf, (**b**) biochar, (**c**) magnetic biochar, and (**d**) the spent magnetic biochar after adsorption test.

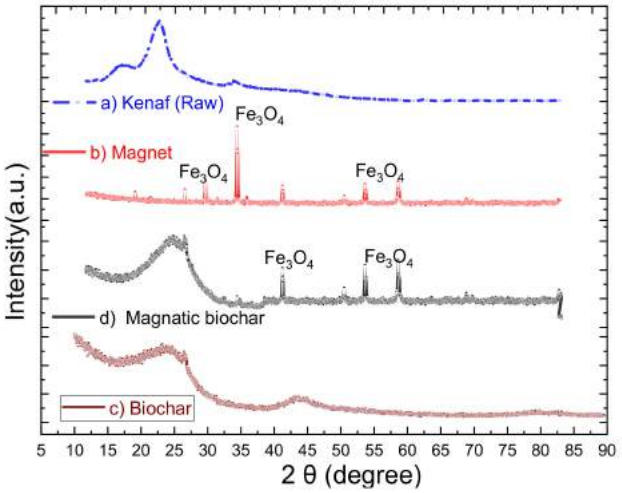

Figure 6. XRD patterns of (**a**) kenaf (raw), (**b**) Fe_3O_4, (**c**) biochar, and (**d**) magnetic biochar.

3.1.5. Surface Functional Group

Figure 7 shows the FTIR spectra indicating that adsorption of metals on the surface of biochar is influenced by the pyrolysis temperature, the raw materials used, and the activation agent, as also reported elsewhere [75]. Figure 7c shows that there was an improvement due to pyrolysis temperature indicated by a peak at 1483 cm^{-1} corresponding to the C=O bonds and aromatic hydrocarbon. The broad and strong peak at 3440 cm^{-1}

indicates the O–H bond. Meanwhile, the peak at 1375 cm^{-1} represents the C=C bond. The peak at 675 cm^{-1} represents the C–H bending.

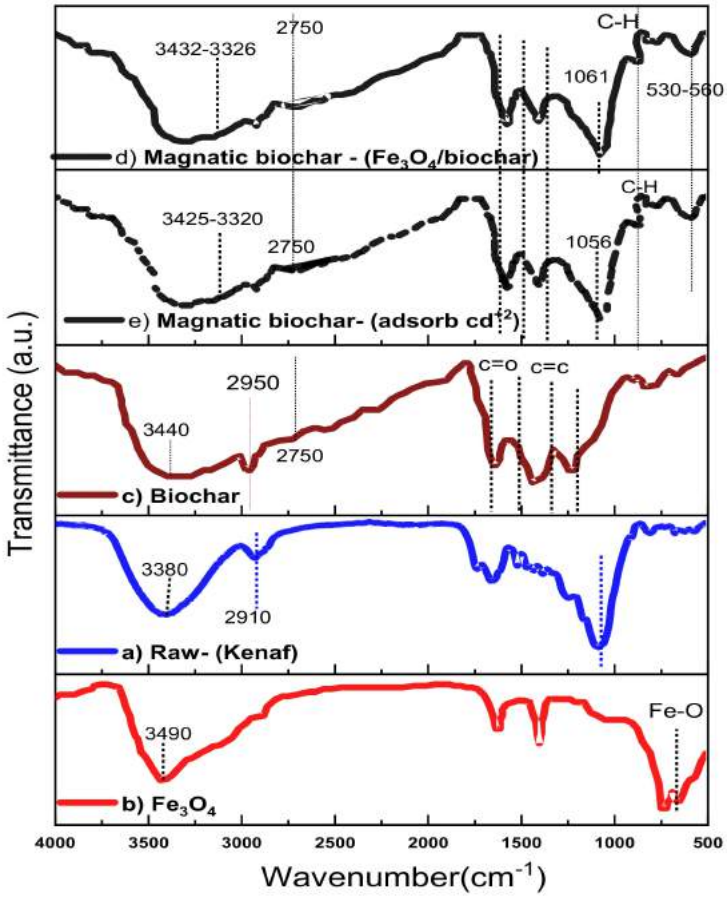

Figure 7. FTIR spectra of (**a**) kenaf (raw), (**b**) Fe_3O_4, (**c**) biochar, (**d**) magnetic biochar, and (**e**) magnetic biochar (after Cd(II) adsorption).

Magnetic biochar in Figure 7d,f show the stretching vibration of hydroxyl (O–H) at 3320 cm^{-1}–3425 cm^{-1} and 3325 cm^{-1}–3432 cm^{-1}, respectively [76]. Similarly, the magnetic biochars have stretching vibration of lactone, carbonyl, ester, carboxylic, and aromatic structure (C=O) at 1615 cm^{-1}–1580 cm^{-1}. The peak at 3320 cm^{-1}–3425 cm^{-1} for the magnetic biochar significantly weakened after adsorption, where there was a significant shift from 3320 cm^{-1}–3425cm^{-1} to 3325 cm-^{1}–3432 cm^{-1} and that shift occurred due to the interaction between Cd(II) and hydroxyl groups which formed on the magnetic biochar [77]. The magnetic biochar has the highest number of pores and high peaks ranging from 530 cm^{-1} to 560 cm^{-1}, indicating the presence of Fe particles on its surface. Furthermore, the broad stretching vibration peaks ranged from 2750 cm^{-1}–2950 cm^{-1} could be the C–H groups of nonionic carboxylic groups, while peaks at 1650 cm^{-1}–1700 cm^{-1} indicated the presence of C=O groups as a result of the pyrolysis process [78,79].

3.1.6. XPS Analysis

Figures 8–10 show the XPS spectra of the biochar, the magnetic biochar, and the spent magnetic biochar, respectively. The figures show the XPS high-resolution spectra of C1s, O1s, Fe2p, and Cdp2 spectrum regions on the adsorbents. Figure 8a,b and Figure 9a,b show the region of C1s spectrum and O1s spectrum indicating that the presence of carbon with little oxygen in the pristine biochar increases the oxygen and presence of Fe after impregnation with Fe_3O_4. Figure 8a shows that there was a significant difference with carbon-containing group peaks observed for the carbon peaks of the biochar. As shown at 284 eV in Figure 8a, carbon was bound to carbon and hydrogen; at 284.68 eV, carbon was

bound to oxygen or nitrogen (carbonyl, amines, alcohols, or amides); at 287.7 eV, carbon formed two single bonds or one double bond with oxygen (acetals, amides, carboxylates, hemiacetals, and acetals); at 292.6 eV, carbon formed one double bond and one single bond with oxygen (carboxyl group). Similarly, in Figure 8b, the O1s peaks revealed oxygen-containing groups, with the existence of O=C, C–O, C=O, and O–H confirmed by the XPS spectrum of O1s at 536, 533.6, 531.2, and 530.60 eV, respectively.

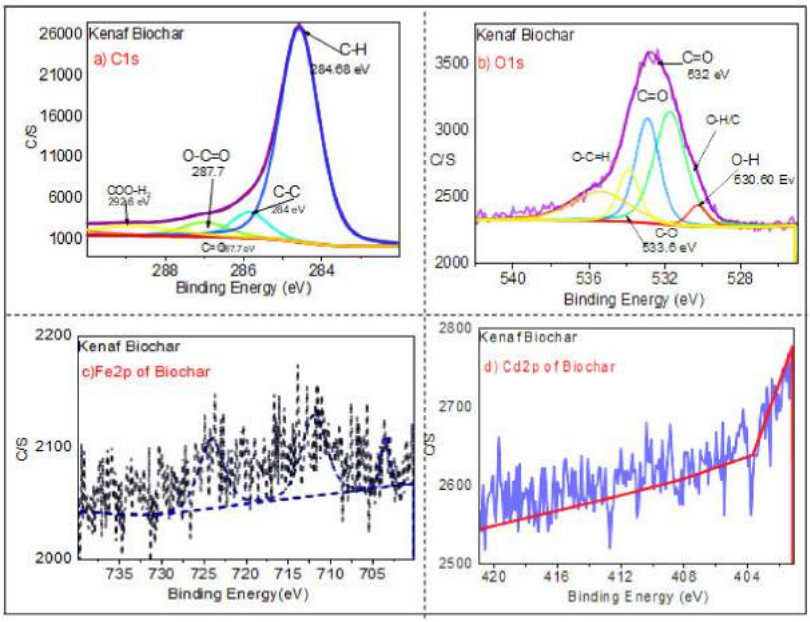

Figure 8. XPS analysis of the biochar by showing (**a**) C1s spectrum, (**b**) O1s spectrum, (**c**) Fe2p spectrum, and (**d**) Cdp2 spectrum.

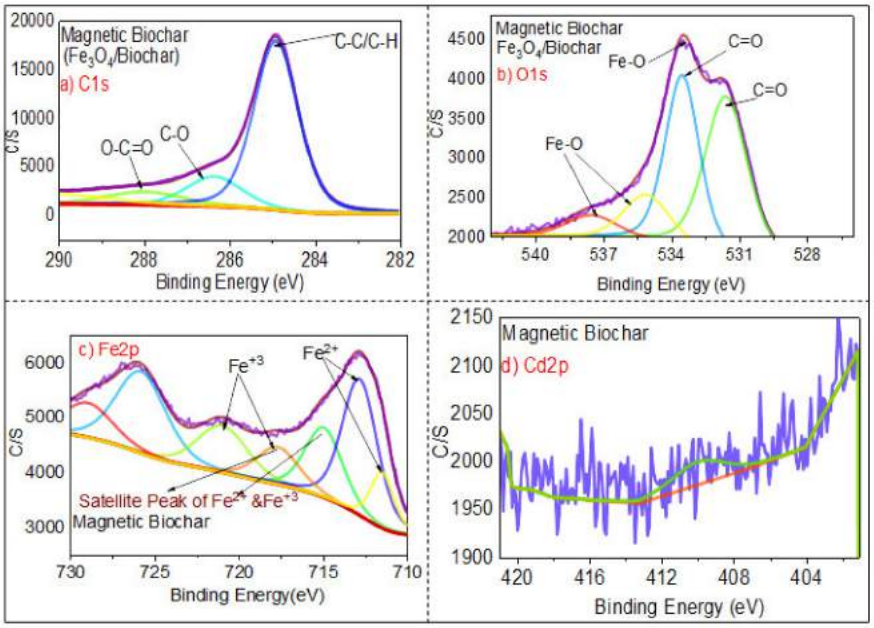

Figure 9. XPS analysis of the magnetic biochar by showing (**a**) C1s spectrum, (**b**) O1s spectrum, (**c**) Fe2p spectrum, and (**d**) Cdp2 spectrum.

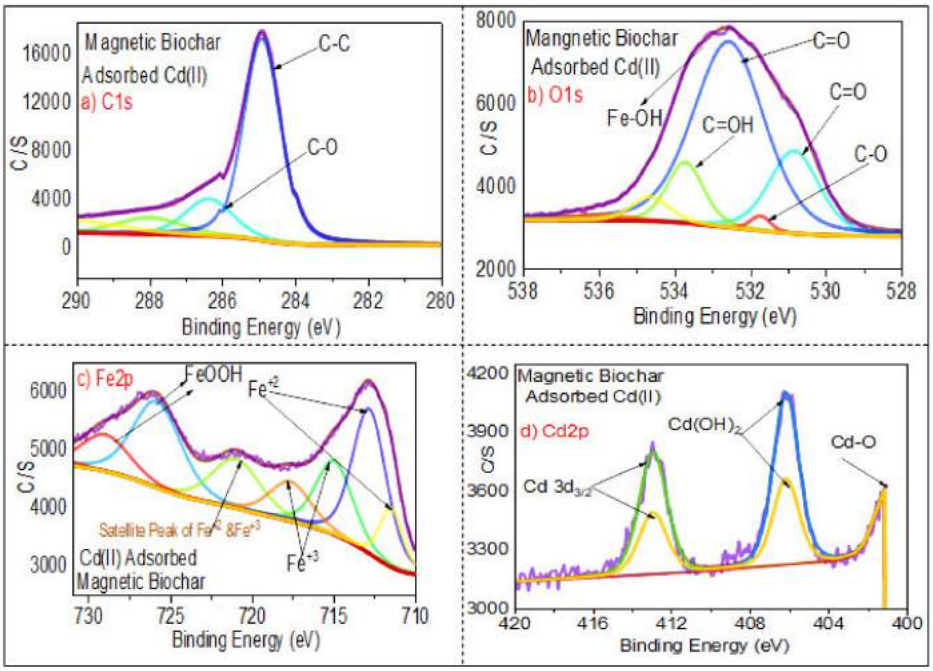

Figure 10. XPS analysis of the spent magnetic biochar by showing (**a**) C1s spectrum, (**b**) O1s spectrum, (**c**) Fe2p spectrum, and (**d**) Cdp2 spectrum.

Figure 9 shows the XPS analysis of magnetic biochar spectra C1s spectrum, O1s spectra, Fe2p spectrum, and Cdp2 spectrum. The C1s spectrum and O1s spectra indicate that the carbon percentage decreased and oxygen percentage increased after the impregnation of biochar with iron. Figure 9c displays XPS spectra with high resolution, revealing the existence of $Fe2p_{1/2}$ at 715.5–725 eV and Fe $2p_{2/3}$ at 711–714.5 eV. These findings demonstrate the presence of Fe^{3+} and Fe^{2+}, which appeared as a result of mixing biochar with iron oxide. Satellite peaks of Fe^{3+} and Fe^{2+} were found at the range of binding energy of 715–720 eV, which is similar to the results of Naeemeh et al. [80] and Haixia Wu et al. [81]. Figure 10c shows that after adsorption of Cd(II), there was a significant displacement of Fe 2p binding energy, implying the occurrence of coordination reactions between Fe and Cd.

Figure 10 shows the broad peaks of magnetic biochar (after adsorption), C1s spectrum, O1s spectrum, Fe2p spectrum, and Cdp2 spectrum. In comparison to the O1s spectrum of the pristine biochar (Figure 8b) showing the presence of oxygen in the form of organic oxygen (C–OH)/C–O–C) and inorganic oxygen (Fe–O/Cd–O), Figure 10b shows strong peaks in the O1s region, indicating several chemical states of oxygen such as organic oxygen (C–OH)/C–O–C) and inorganic oxygen (Fe–O/Cd–(C–O–C). Meanwhile, Figure 10d shows that the Cd 3d3/2 core-level spectrum has two peak components with binding energies of about 413.5 eV, 406 eV, and 402 eV, which can be attributed to Cd–O and Cd $(OH)_2$ species, respectively. The findings show that Cd(II) deposition and chelation played a significant role in the adsorption mechanism [82].

3.2. Adsorption Kinetic Analysis

The kinetics study was applied to Cd^{2+} adsorption using the biochar and the magnetic biochar. Figure 11 shows the evolution of adsorption as function of time under initial Cd^{2+} concentrations (of 5, 10, 20, 40, 60, 80, and 100 mg L^{-1}). The Cd^{2+} adsorption onto the biochar and the magnetic biochar rapidly improve in the first two hours but at different rates. The adsorption on the magnetic biochar in the first two hours reaches double the adsorption on the biochar. Overall understanding from Figure 11 indicated that most of the Cd^{2+} ions could be adsorbed within 4 h until reaching the equilibrium when the internal active adsorption sites were fully occupied. The magnetic biochar adsorbed Cd^{2+} more than the biochar, even in the same period, suggesting that it had better adsorption properties

than the biochar. The surface area and pore volume of magnetic biochar was greater than the surface area and pore volume of biochar of 175.55 m^2 g^{-1}, 0.102366 cm^3 g^{-1}, and 117.70 m^2 g^{-1}, 0.063884 cm^3 g^{-1}, respectively.

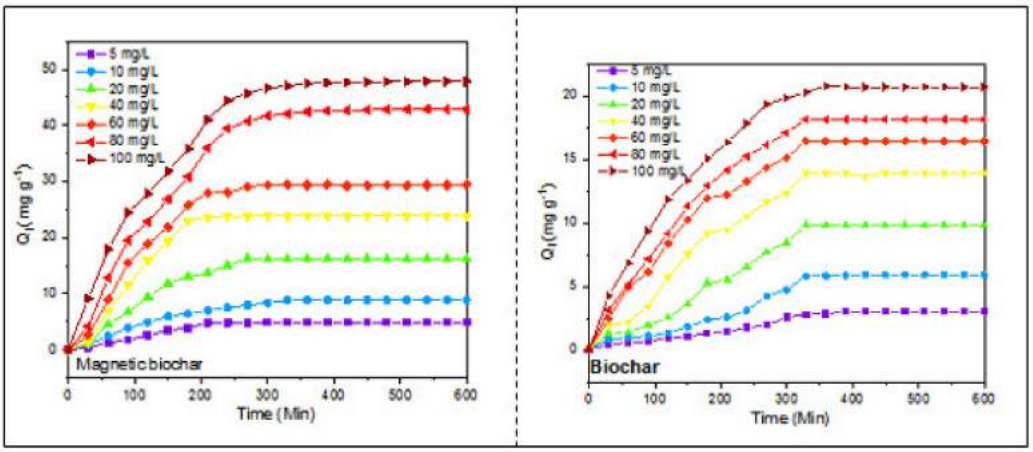

Figure 11. Adsorption kinetics of Cd^{2+} with biochar and magnetic biochar.

The adsorption kinetic characteristics for biochar and magnetic biochar onto cadmium adsorption are shown in Figure S1 and Table S1 (Supplementary Materials). The pseudo-first-order model has a lower correlation coefficient than the pseudo-second-order model, indicating that the latter fits better to explain the adsorption kinetic which associates with the chemisorption mechanism. Furthermore, the calculated adsorption capacity values with the pseudo-second-order model were close to ones obtained from the experiments, which confirmed the good fittings of the pseudo-second-order model.

Table S1 shows that the pseudo-second-order model is more suitable for the rate-determining step than the pseudo-first-order model, which is comparable to the study by Chowdhury et al. [83], and includes valence forces from the exchange or sharing of electrons between the adsorbate and adsorbent. The estimated value of Q_{cal} using the pseudo-second-order model was close to the experimental value, confirming the pseudo-second-order model's ability to fit the kinetic adsorption data. The adsorption capacity constant (K_2) of magnetic biochar was higher than the adsorption capacity constant of pristine biochar (K_2), indicating that fast sorption of Cd^{2+} to magnetic biochar where K_2 values at initial concentration 100 ppm for magnetic biochar and pristine biochar were 0.127 (g/mg.min) and 0.025 (g/mg.min), respectively.

3.3. Adsorption Isotherm Analysis

The adsorption isotherms of treatment of Cd^{2+}-containing solutions were successfully determined using experimental adsorption results by linearly fitting models of Temkin, Freundlich, and Langmuir. The analysis of adsorption isotherms is very important for understanding the mechanism of the adsorption process and the principle and mathematical derivation of adsorption characteristics. The result of isotherm analysis is shown in Figure S2 and Table S2 (Supplementary file). The maximum R^2 values of the tested isotherms indicated that the model mostly suits the experimental results [2,84]. Comparing the correlation coefficients for the three isotherm models obtained for biochar and magnetic biochar, the most suitable is the Langmuir model. It shows that the magnetic biochar had superior adsorption ability than the biochar due to its higher surface area, stronger affinity toward Cd^{2+}, and a larger number of actives sites. The K_L of the magnetic biochar of 0.09798 L mg^{-1} is higher than the K_L of the biochar of 0.035196 L mg^{-1}. It confirms the stronger affinity of magnetic biochar to the Cd^{2+} [85]. The high adsorption capacity of magnetic biochar might be due to the good affinity of cadmium to iron oxide on the magnetic biochar, which was also presented by XPS characterization, which generates a stable inner sphere to the surface functional groups(–COOH, –OH) [86]. In Table S2, it is

proved that the Langmuir isotherm model fits well, with a correlation R^2 value of 0.963 and 0.995 for both biochar and magnetic biochar, respectively, while the Freundlich and Temkin isotherm model correlation R^2 values for biochar and magnetic biochar were 0.953, 0.983, 0.773, and 0.913, respectively.

3.4. Effect of pH

pH is one of the significant parameters that influence the adsorption capacity. The adsorption capacity might be influenced by pH in different aspects: concentration of metal ions or electrical surface charge on the adsorption [87,88]. The range of pH was between 2.0–10 to study the influence of pH on adsorption capacity, while the other parameters were kept constant. Figure 12a shows the effect of the solution pH on the adsorption of Cd^{2+} on the magnetic biochar and the biochar. The trend indicated that the adsorption capacity for both adsorbents increases as pH increased to 6, then it slightly decreased. The adsorption capacity of magnetic biochar and biochar was 9.65 mg g^{-1} and 21.1 mg g^{-1}, respectively, at pH 2.0, and later reached the maximum value of 43.92 mg g^{-1} and 22 mg g^{-1}, respectively, at pH value 6.0. The high adsorption capacity of adsorbents on cadmium ions occurred around pH ranging from 5.5 to 6.0. This happened because the surface of biochar becomes saturated with hydrogen ions at lower pH levels, and this saturation prevents the removal of cadmium ions owing to the mutual repulsion between cadmium and hydrogen ions [89,90]. Above pH 6.0, cadmium precipitation usually occurs. This is because insoluble cadmium hydroxides such as Cd $(OH)_2$ and Cd $(OH)^{3-}$ begin to precipitate out of solution at higher pH values. This must be avoided to discriminate between sorption and precipitation [90].

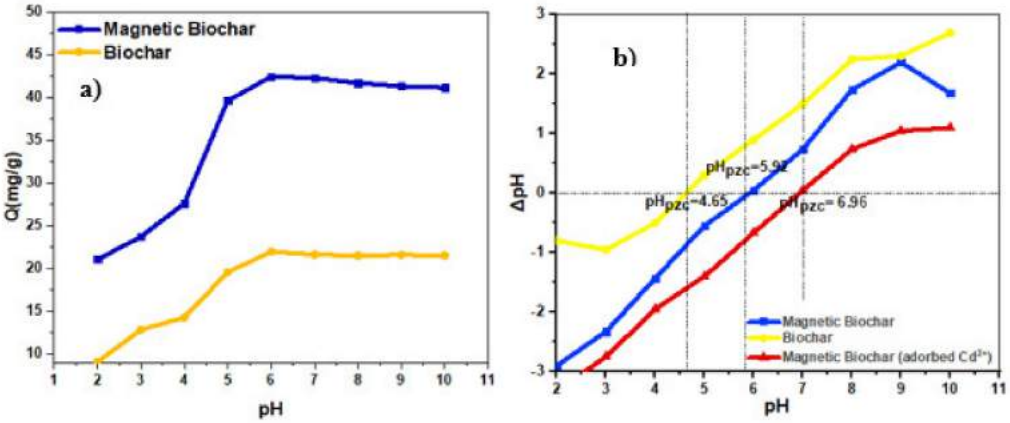

Figure 12. (**a**) Effect of solution pH on adsorption capacity of biochar and magnetic biochar and (**b**) point-of-zero charges of biochar, magnetic biochar, and magnetic biochar (adsorbed Cd^{2+}).

The results of this study agree with the ones obtained by Usman et al. [91], which stated that the adsorption capacity increased with increased pH solution. This might be attributed to a lower level of competition between protons and Cd^{2+} for accessible sorption sites. Furthermore, as pH rises, the number of binding sites increases, hence increasing metal adsorption on the adsorbent surface. Figure 12b shows the pH_{PZC} result which indicated that the pH_{pzc} of magnetic biochar was 6.92. If pH_{pzc} > pH, the adsorption capacity might be reduced due to possible electrostatic repulsion between the positive change of magnetic biochar and the positive charge of cadmium ions. Figure 12b shows that after adsorption, the magnetic biochar changed toward the positive, indicating that the cadmium ions were efficiently adsorbed as inner-sphere surface complexes or cations that may neutralize the surface's negative charge [59,92].

3.5. Effect of Temperature

Thermodynamic adsorption study is crucial because it determines whether the adsorption process is a spontaneous process or an intended process. The enthalpy (ΔH°), entropy (ΔS°), and change in Gibbs free energy (ΔG°) were calculated based on the following equations:

$$\Delta G^\circ = -RTInK_L \quad (3)$$

$$\Delta G^\circ = \Delta H^\circ - T\Delta S^\circ \quad (4)$$

Table 3 shows the thermodynamic parameters of Cd^{2+} adsorption using the magnetic biochar at different temperatures. It proves that the adsorption process was spontaneous and endothermic, with negative values of Gibbs free energy (ΔG°) and positive values of ΔH° and ΔS°. Such a mechanism is thermodynamically feasible and conforms to a chemical reaction in Cd^{2+} adsorption because the ΔG° is negative. Additionally, when the ΔG° reduced, the temperature climbed (−3.96, −4.42, and −4.70 kJ mol^{-1}), showing that the feasibility rose with temperature. The temperature affects the Cd^{2+} adsorption of magnetic biochar, as demonstrated in Figure S3, which proves that ion mobility increases with increasing temperature.

Table 3. Thermodynamic parameters of Cd^{2+} adsorption on the magnetic biochar at different temperatures.

T(K)	Q_e (mg g^{-1})	InK_L	ΔG° (KJ mole $^{-1}$)	ΔH° (kJ mole $^{-1}$)	ΔS° (KJ mole $^{-1}$)
298	44.60	1.60	−3.96	8.69	0.042
308	45.80	1.73	−4.42		
318	47.30	1.82	−4.70		

3.6. Performance Assessment of Magnetic Biochar in Comparison with Literature

Table 4 shows the performance of magnetic biochar for Cd^{2+} adsorption compared to magnetic adsorbents reported in the literature. The adsorption capacity of magnetic biochars for Cd^{2+} ranges from 6.34 to 197.76 mg/g [93]. The adsorption capacity of Fe_3O_4/kenaf fiber biochar for Cd^{2+} adsorption is better than the magnetic oak wood biochar, magnetic coconut shell biochar, magnetic Douglas fir biochar, and other magnetic adsorbents. However, the adsorption capacity of chitosan-modified magnetic biochar composite is higher than that of Fe_3O_4/kenaf fiber biochar. The performance comparison results indicated and reconfirmed that magnetic biochar composites from the kenaf with Fe_3O_4 are positively capable of being an efficient adsorbent for cadmium removal from aqueous environments.

Table 4. Performance of magnetic biochar for Cd^{2+} adsorption compared to literature-based magnetic adsorbents.

Adsorbent	SSA (m^2 g^{-1})	pH	Cd^{2+} Adsorption Capacity (mg g^{-1})	Ref.
Magnetic oak wood biochar	8.80	5	7.40	[94]
(iron oxide/tangerine peel biochar)	-	4	15.5	[95]
Magnetic coconut shell biochar	834	4.8	4.77	[96]
Magnetic spent coffee ground biochar	3.60	7	10.42	[97]
Magnetic hollow porous oval shape $NiFe_2O_4$	-	5	16.65	[98]
Grape husk/$FeSO_4.7H_2O$	127	5	38.3	[99]
Algal-magnetic biochar	63.33	5	19.40	[100]
Fe_3O_4@$FePO_4$	-	7	13.51	[49]
Magnetic Douglas fir biochar	460	5	11	[58]
(Mangosteen peel/Fe_2o_3) biochar	-	7	45.662	[101]
Magnetic chicken manure biochar	5.44	6	8.1	[102]
Chitosan modified magnetic biochar composite	112.33	6	93.72	[103]
Corn straw waste @ferric nitrate	313.90	2–10	46.15	[59]
Fly ash/Fe_3O_4	-	5	9.65	[104]
Fe_3O_4/kenaf fiber biochar	175.55	6	47.90	This study

4. Conclusions

The magnetic biochar derived from kenaf fiber showed better performance than pristine biochar, with twice-higher adsorption capacity. The magnetic biochar demonstrated enormous physicochemical properties such as surface area, pore volume, more oxygen-containing functional groups, and fine pore structure. The magnetic biochar offers a high adsorption capacity of Cd^{2+}. The adsorption process was favored at 5–6 pH values. The Langmuir model best suited the experimental data with the correlation coefficient R^2 of >0.99, compared to other models. The R^2 for the pseudo-second-order model was higher than the pseudo-first-order model for all tested initial Cd^{2+} concentrations, implying predominance of the chemical adsorption process. The overall results suggest that magnetic biochar is fully suited for Cd^{2+} removal. Further study can focus on the magnetic induced separation of the magnetic adsorbent using an external magnetic field.

Supplementary Materials: The following are available online at https://www.mdpi.com/article/10.3390/ijerph18157949/s1, Figure S1: Adsorption kinetic parameters for the biochar and magnetic biochar –Cd^{2+} adsorption system, Table S1: Isotherm parameter of Cd^{2+} adsorption with biochar and magnetic biochar, Figure S1: Kinetic models of the (a) pseudo-first order and (b) pseudo-second order, Figure S2: Fitting of isotherm models: (a) Langmuir isotherm, (b) Freundlich isotherm, and (c) Temkin isotherm, Figure S3: Influence of temperature on Cd^{2+} adsorption by magnetic biochar.

Author Contributions: Conceptualization, A.A.H.S., N.Y.H., and S.S.; methodology, A.A.H.S. and N.Y.H.; software, A.A.H.S. and A.A.S.G.; validation, A.A.H.S., M.R.B., and N.Y.H.; formal analysis, A.A.H.S. and Z.Y.Z.; investigation, A.A.H.S., A.H.J., and H.G.M.; resources, A.A.H.S. and N.Y.H.; data curation, A.A.H.S.; writing—original draft preparation, A.A.H.S. and M.R.B.; writing—review and editing, M.R.B. and A.H.J.; visualization, A.A.S.G. and H.G.M.; supervision, N.Y.H. and S.S.; project administration, A.A.H.S. and N.Y.H.; funding acquisition, N.Y.H. All authors have read and agreed to the published version of the manuscript.

Funding: This work was funded by the Yayasan Universiti Teknologi PETRONAS (YUTP) with grant code YUTP-015LC0-210.

Institutional Review Board Statement: Not applicable.

Informed Consent Statement: Informed consent was obtained from all subjects involved in the study.

Data Availability Statement: The data presented in this study are available from the corresponding author upon reasonable request.

Acknowledgments: The authors would like to thank Universiti Teknologi PETRONAS for funding this study. The authors are grateful to the participants who contributed to the research as well.

Conflicts of Interest: The authors declare no conflict of interest.

References

1. Sayed, M.; Tabassum, S.; Shah, N.S.; Khan, J.A.; Shah, L.A.; Rehman, F.; Khan, S.U.; Khan, H.M.; Ullah, M. Acid fuchsin dosimeter: A potential dosimeter for food irradiation dosimetry. *J. Food Meas. Charact.* **2018**, *13*, 707–715. [CrossRef]
2. Saeed, A.; Harun, N.; Sufian, S.; Siyal, A.; Zulfiqar, M.; Bilad, M.; Vagananthan, A.; Al-Fakih, A.; Ghaleb, A.; Almahbashi, N. *Eucheuma cottonii* Seaweed-Based Biochar for Adsorption of Methylene Blue Dye. *Sustainability* **2020**, *12*, 10318. [CrossRef]
3. Jagaba, A.H.; Abubakar, S.; Nasara, M.A.; Jagaba, S.M.; Chamah, H.M.; Lawal, I.M. Defluoridation of Drinking Water by Activated Carbon Prepared from Tridax Procumbens Plant (A Case Study of Gashaka Village, Hong L. G. A., Adamawa State, Nigeria). *Int. J. Comput. Theor. Chem.* **2019**, *7*, 1. [CrossRef]
4. Waalkes, M.P. Cadmium carcinogenesis in review. *J. Inorg. Biochem.* **2000**, *79*, 241–244. [CrossRef]
5. Saeed, A.A.H.; Harun, N.Y.; Nasef, M.M.; Afolabi, H.K.; Ghaleb, A.A.S. Removal of Cadmium from Aqueous Solution by Optimized Magnetic Biochar Using Response Surface Methodology. *ICCOEE 2021* **2021**, 119–126. [CrossRef]
6. Bernhoft, R.A. Cadmium Toxicity and Treatment. *Sci. World J.* **2013**, *2013*, 1–7. [CrossRef]
7. Pyrzynska, K. Removal of cadmium from wastewaters with low-cost adsorbents. *J. Environ. Chem. Eng.* **2019**, *7*, 102795. [CrossRef]
8. Godt, J.; Scheidig, F.; Grosse-Siestrup, C.; Esche, V.; Brandenburg, P.; Reich, A.; Groneberg, D. The toxicity of cadmium and resulting hazards for human health. *J. Occup. Med. Toxicol.* **2006**, *1*, 1–6. [CrossRef] [PubMed]
9. Genchi, G.; Sinicropi, M.S.; Lauria, G.; Carocci, A.; Catalano, A. The Effects of Cadmium Toxicity. *Int. J. Environ. Res. Public Health* **2020**, *17*, 3782. [CrossRef]

10. Kavand, M.; Eslami, P.; Razeh, L. The adsorption of cadmium and lead ions from the synthesis wastewater with the activated carbon: Optimization of the single and binary systems. *J. Water Process. Eng.* **2020**, *34*, 101151. [CrossRef]
11. Hezam Saeed, A.A.; Harun, N.Y.; Sufian, S.; Bin Aznan, M.F. Effect of Adsorption Parameter on the Removal of Nickel (II) by Low-Cost Adsorbent Extracted From Corn Cob. *Int. J. Adv. Res. Eng. Technol.* **2020**, *11*, 981–989.
12. Chowdhury, P.; Elkamel, A.; Ray, A.K. Photocatalytic Processes for the Removal of Toxic Metal Ions. *Heavy Met. Water Presence Remov. Saf.* **2014**, 25–43. [CrossRef]
13. Zhang, S.; Cui, M.; Chen, J.; Ding, Z.; Wang, X.; Mu, Y.; Meng, C. Modification of synthetic zeolite X by thiourea and its adsorption for Cd (II). *Mater. Lett.* **2019**, *236*, 233–235. [CrossRef]
14. Saeed, A.A.H.; Saimon, N.N.; Ali, M.W.; Kidam, K.; Jusoh, Y.M.; Jusoh, M.; Zakaria, Z.Y. Effect of particle size on the explosive characteristics of grain (Wheat) starch in a closed cylindrical vessel. *Chem. Eng. Trans.* **2018**, *63*, 571–576. [CrossRef]
15. Rout, P.R.; Zhang, T.C.; Bhunia, P.; Surampalli, R.Y. Treatment technologies for emerging contaminants in wastewater treatment plants: A review. *Sci. Total. Environ.* **2021**, *753*, 141990. [CrossRef] [PubMed]
16. Zamri, M.F.M.A.; Kamaruddin, M.A.; Yusoff, M.S.; Aziz, H.A.; Foo, K.Y. Semi-aerobic stabilized landfill leachate treatment by ion exchange resin: Isotherm and kinetic study. *Appl. Water Sci.* **2015**, *7*, 581–590. [CrossRef]
17. Bogusz, A.; Oleszczuk, P. Effect of biochar addition to sewage sludge on cadmium, copper and lead speciation in sewage sludge-amended soil. *Chemosphere* **2020**, *239*, 124719. [CrossRef]
18. Jagaba, A.H.; Kutty, S.R.M.; Hayder, G.; Baloo, L.; Ghaleb, A.A.S.; Lawal, I.M.; Abubakar, S.; Al-dhawi, B.N.S.; Almahbashi, N.M.Y.; Umaru, I. Degradation of Cd, Cu, Fe, Mn, Pb and Zn by Moringa-oleifera, zeolite, ferric-chloride, chitosan and alum in an industrial effluent. *Ain Shams Eng. J.* **2020**, *12*, 57–64. [CrossRef]
19. Al-Mekhlafi, A.-B.; Isha, A.; Chileshe, N.; Abdulrab, M.; Saeed, A.; Kineber, A. Modelling the Relationship between the Nature of Work Factors and Driving Performance Mediating by Role of Fatigue. *Int. J. Environ. Res. Public Health* **2021**, *18*, 6752. [CrossRef]
20. Renu; Agarwal, M.; Singh, K. Methodologies for removal of heavy metal ions from wastewater: An overview. *Interdiscip. Environ. Rev.* **2017**, *18*, 124–142. [CrossRef]
21. Baloo, L.; Isa, M.H.; Bin Sapari, N.; Jagaba, A.H.; Wei, L.J.; Yavari, S.; Razali, R.; Vasu, R. Adsorptive removal of methylene blue and acid orange 10 dyes from aqueous solutions using oil palm wastes-derived activated carbons. *Alex. Eng. J.* **2021**, *60*, 5611–5629. [CrossRef]
22. Akhil, D.; Lakshmi, D.; Kartik, A.; Vo, D.-V.N.; Arun, J.; Gopinath, K.P. Production, characterization, activation and environmental applications of engineered biochar: A review. *Environ. Chem. Lett.* **2021**, *19*, 2261–2297. [CrossRef]
23. Kılıç, M.; Çepelioğullar; Pütün, A.E. Adsorption of heavy metal ions from aqueous solutions by bio-char, a by-product of pyrolysis. *Appl. Surf. Sci.* **2013**, *283*, 856–862. [CrossRef]
24. Inyang, M.I.; Gao, B.; Yao, Y.; Xue, Y.; Zimmerman, A.; Mosa, A.; Pullammanappallil, P.; Ok, Y.S.; Cao, X. A review of biochar as a low-cost adsorbent for aqueous heavy metal removal. *Crit. Rev. Environ. Sci. Technol.* **2015**, *46*, 406–433. [CrossRef]
25. Komkiene, J.; Baltrenaite, E. Biochar as adsorbent for removal of heavy metal ions [Cadmium (II), Copper (II), Lead (II), Zinc (II)] from aqueous phase. *Environ. Sci. Technol.* **2016**, *13*, 471–482. [CrossRef]
26. Harun, N.Y.; Han, T.J.; Vijayakumar, T.; Saeed, A.; Afzal, M. Ash Deposition Characteristics of Industrial Biomass Waste and Agricultural Residues. *Mater. Today Proc.* **2019**, *19*, 1712–1721. [CrossRef]
27. Tripathi, M.; Sahu, J.N.; Ganesan, P. Effect of process parameters on production of biochar from biomass waste through pyrolysis: A review. *Renew. Sustain. Energy Rev.* **2016**, *55*, 467–481. [CrossRef]
28. Saeed, A.A.H.; Harun, N.Y.; Nasef, M.M. Physicochemical characterization of different agricultural residues in malaysia for bio char production. *Int. J. Civ. Eng. Technol.* **2019**, *10*, 213–225.
29. Saeed, A.A.H.; Harun, N.Y.; Sufian, S.; Afolabi, H.K.; Al-Qadami, E.H.H.; Roslan, F.A.S.; Rahim, S.A.; Ghaleb, A.A.S. Production and Characterization of Rice Husk Biochar and Kenaf Biochar for Value-Added Biochar Replacement for Potential Materials Adsorption. *Ecol. Eng. Env. Tech.* **2021**, *22*, 1–8.
30. Yi, Y.; Tu, G.; Zhao, D.; Tsang, P.E.; Fang, Z. Biomass waste components significantly influence the removal of Cr(VI) using magnetic biochar derived from four types of feedstocks and steel pickling waste liquor. *Chem. Eng. J.* **2019**, *360*, 212–220. [CrossRef]
31. Thompson, K.; Shimabuku, K.K.; Kearns, J.; Knappe, D.; Summers, R.S.; Cook, S.M. Environmental Comparison of Biochar and Activated Carbon for Tertiary Wastewater Treatment. *Environ. Sci. Technol.* **2016**, *50*, 11253–11262. [CrossRef] [PubMed]
32. Qambrani, N.A.; Rahman, M.; Won, S.; Shim, S.; Ra, C. Biochar properties and eco-friendly applications for climate change mitigation, waste management, and wastewater treatment: A review. *Renew. Sustain. Energy Rev.* **2017**, *79*, 255–273. [CrossRef]
33. Song, Z.; Lian, F.; Yu, Z.; Zhu, L.; Xing, B.; Qiu, W. Synthesis and characterization of a novel MnOx-loaded biochar and its adsorption properties for Cu^{2+} in aqueous solution. *Chem. Eng. J.* **2014**, *242*, 36–42. [CrossRef]
34. Regmi, P.; Moscoso, J.L.G.; Kumar, S.; Cao, X.; Mao, J.; Schafran, G. Removal of copper and cadmium from aqueous solution using switchgrass biochar produced via hydrothermal carbonization process. *J. Environ. Manag.* **2012**, *109*, 61–69. [CrossRef]
35. Park, J.-H.; Wang, J.; Kim, S.-H.; Kang, S.-W.; Jeong, C.Y.; Jeon, J.-R.; Park, K.H.; Cho, J.-S.; Delaune, R.D.; Seo, D.-C. Cadmium adsorption characteristics of biochars derived using various pine tree residues and pyrolysis temperatures. *J. Colloid Interface Sci.* **2019**, *553*, 298–307. [CrossRef]
36. Kołodyńska, D.; Wnętrzak, R.; Leahy, J.J.; Hayes, M.; Kwapiński, W.; Hubicki, Z. Kinetic and adsorptive characterization of biochar in metal ions removal. *Chem. Eng. J.* **2012**, *197*, 295–305. [CrossRef]

37. Xu, X.; Cao, X.; Zhao, L. Comparison of rice husk- and dairy manure-derived biochars for simultaneously removing heavy metals from aqueous solutions: Role of mineral components in biochars. *Chemosphere* **2013**, *92*, 955–961. [CrossRef]
38. Mohan, D.; Pittman, C.U.; Bricka, M.; Smith, F.; Yancey, B.; Mohammad, J.; Steele, P.H.; Franco, M.A.; Gómez-Serrano, V.; Gong, H. Sorption of arsenic, cadmium, and lead by chars produced from fast pyrolysis of wood and bark during bio-oil production. *J. Colloid Interface Sci.* **2007**, *310*, 57–73. [CrossRef]
39. Ma, F.; Zhao, B.; Diao, J. Adsorption of cadmium by biochar produced from pyrolysis of corn stalk in aqueous solution. *Water Sci. Technol.* **2016**, *74*, 1335–1345. [CrossRef] [PubMed]
40. Zhang, H.; Yue, X.; Li, F.; Xiao, R.; Zhang, Y.; Gu, D. Preparation of rice straw-derived biochar for efficient cadmium removal by modification of oxygen-containing functional groups. *Sci. Total. Environ.* **2018**, *631–632*, 795–802. [CrossRef]
41. Gupta, S.; Sireesha, S.; Sreedhar, I.; Patel, C.M.; Anitha, K. Latest trends in heavy metal removal from wastewater by biochar based sorbents. *J. Water Process. Eng.* **2020**, *38*, 101561. [CrossRef]
42. Sizmur, T.; Fresno, T.; Akgül, G.; Frost, H.; Moreno-Jiménez, E. Biochar modification to enhance sorption of inorganics from water. *Bioresour. Technol.* **2017**, *246*, 34–47. [CrossRef]
43. Petrović, J.; Stojanović, M.; Milojković, J.V.; Petrović, M.; Šoštarić, T.; Laušević, M.D.; Mihajlović, M.L. Alkali modified hydrochar of grape pomace as a perspective adsorbent of Pb $^{2+}$ from aqueous solution. *J. Environ. Manag.* **2016**, *182*, 292–300. [CrossRef]
44. Saeed, A.A.H.; Harun, N.Y.; Zulfani, N. Heavy Metals Capture from Water Sludge by Kenaf Fibre Activated Carbon in Batch Adsorption. *J. Ecol. Eng.* **2020**, *21*, 102–115. [CrossRef]
45. Gwenzi, W.; Chaukura, N.; Noubactep, C.; Mukome, F.N. Biochar-based water treatment systems as a potential low-cost and sustainable technology for clean water provision. *J. Environ. Manag.* **2017**, *197*, 732–749. [CrossRef] [PubMed]
46. Saeed, A.; Harun, N.Y.; Bilad, M.; Afzal, M.; Parvez, A.; Roslan, F.; Rahim, S.A.; Vinayagam, V.; Afolabi, H. Moisture Content Impact on Properties of Briquette Produced from Rice Husk Waste. *Sustainability* **2021**, *13*, 3069. [CrossRef]
47. Rajapaksha, A.U.; Chen, S.S.; Tsang, D.C.; Zhang, M.; Vithanage, M.; Mandal, S.; Gao, B.; Bolan, N.S.; Ok, Y.S. Engineered/designer biochar for contaminant removal/immobilization from soil and water: Potential and implication of biochar modification. *Chemosphere* **2016**, *148*, 276–291. [CrossRef]
48. Rizwan, M.; Lin, Q.; Chen, H.; Li, Y.; Li, G.; Zhao, X.; Tian, Y. Synthesis, characterization and application of magnetic and acid modified biochars following alkaline pretreatment of rice and cotton straws. *Sci. Total. Environ.* **2020**, *714*, 136532. [CrossRef] [PubMed]
49. Zhang, X.; Sun, C.; Zhang, L.; Liu, H.; Cao, B.; Liu, L.; Gong, W. Adsorption studies of cadmium onto magnetic Fe_3O_4@$FePO_4$ and its preconcentration with detection by electrothermal atomic absorption spectrometry. *Talanta* **2018**, *181*, 352–358. [CrossRef]
50. Mohammed, H.G.; Albarody, T.M.B.; Mustapha, M.; Sultan, N.; Al-Jothery, H. Investigate the effect of process parameters of magnetic inductively assisted spark plasma sintering (SPS) of iron oxide (Fe_3O_4) on microstructure behaviour—Part I. *Mater. Today Proc.* **2021**, *42*, 2106–2112. [CrossRef]
51. Jagaba, A.H.; Kutty, S.R.M.; Salih, G.H.A.; Noor, A.; Hafiz, M.F.U.B.M.; Yaro, N.S.A.; Saeed, A.A.H.; Lawal, I.M.; Birniwa, A.H.; Kilaco, A.U. Palm Oil Clinker as a Waste by-Product: Utilization and Circular Economy Potential. *IntechOpen* **2021**. [CrossRef]
52. Sun, Y.; Yu, I.K.; Tsang, D.C.; Cao, X.; Lin, D.; Wang, L.; Graham, N.J.; Alessi, D.; Komárek, M.; Ok, Y.S.; et al. Multifunctional iron-biochar composites for the removal of potentially toxic elements, inherent cations, and hetero-chloride from hydraulic fracturing wastewater. *Environ. Int.* **2019**, *124*, 521–532. [CrossRef]
53. Zhao, C.; Wang, B.; Theng, B.K.; Wu, P.; Liu, F.; Wang, S.; Lee, X.; Chen, M.; Li, L.; Zhang, X. Formation and mechanisms of nano-metal oxide-biochar composites for pollutants removal: A review. *Sci. Total. Environ.* **2021**, *767*, 145305. [CrossRef] [PubMed]
54. Mohammed, H.; Albarody, T.; Susilawati, S.; Gohari, S.; Doyan, A.; Prayogi, S.; Bilad, M.; Alebrahim, R.; Saeed, A. Process Optimization of In Situ Magnetic-Anisotropy Spark Plasma Sintering of M-Type-Based Barium Hexaferrite $BaFe_{12}O_{19}$. *Materials* **2021**, *14*, 2650. [CrossRef]
55. Agrafioti, E.; Kalderis, D.; Diamadopoulos, E. Ca and Fe modified biochars as adsorbents of arsenic and chromium in aqueous solutions. *J. Environ. Manag.* **2014**, *146*, 444–450. [CrossRef]
56. Frišták, V.; Micháleková-Richveisová, B.; Víglašová, E.; Ďuriška, L.; Galamboš, M.; Moreno-Jimenéz, E.; Pipíška, M.; Soja, G. Sorption separation of Eu and As from single-component systems by Fe-modified biochar: Kinetic and equilibrium study. *J. Iran. Chem. Soc.* **2017**, *14*, 521–530. [CrossRef]
57. Wang, S.; Gao, B.; Zimmerman, A.; Li, Y.; Ma, L.; Harris, W.G.; Migliaccio, K. Removal of arsenic by magnetic biochar prepared from pinewood and natural hematite. *Bioresour. Technol.* **2015**, *175*, 391–395. [CrossRef]
58. Karunanayake, A.G.; Todd, O.A.; Crowley, M.; Ricchetti, L.; Pittman, C.U.; Anderson, R.; Mohan, D.; Mlsna, T. Lead and cadmium remediation using magnetized and nonmagnetized biochar from Douglas fir. *Chem. Eng. J.* **2018**, *331*, 480–491. [CrossRef]
59. Khan, Z.H.; Gao, M.; Qiu, W.; Islam, S.; Song, Z. Mechanisms for cadmium adsorption by magnetic biochar composites in an aqueous solution. *Chemosphere* **2020**, *246*, 125701. [CrossRef] [PubMed]
60. Saeed, A.; Harun, N.; Sufian, S.; Bilad, M.; Nufida, B.; Ismail, N.; Zakaria, Z.; Jagaba, A.; Ghaleb, A.; Al-Dhawi, B. Modeling and Optimization of Biochar Based Adsorbent Derived from Kenaf Using Response Surface Methodology on Adsorption of Cd^{2+}. *Water* **2021**, *13*, 999. [CrossRef]
61. Wulandari, I.O.; Santjojo, D.J.D.H.; Shobirin, R.A.; Sabarudin, A. Characteristics and magnetic properties of chitosan-coated Fe_3O_4 nanoparticles prepared by ex-situ co-precipitation method. *Rasayan J. Chem.* **2017**, *10*, 1348–1358.

62. Singh, H.; Du, J.; Singh, P.; Mavlonov, G.T.; Yi, T.H. Development of superparamagnetic iron oxide nanoparticles via direct conjugation with ginsenosides and its in-vitro study. *J. Photochem. Photobiol. B Biol.* **2018**, *185*, 100–110. [CrossRef] [PubMed]
63. Bakatula, E.N.; Richard, D.; Neculita, C.M.; Zagury, G.J. Determination of point of zero charge of natural organic materials. *Environ. Sci. Pollut. Res.* **2018**, *25*, 7823–7833. [CrossRef] [PubMed]
64. Langmuir, I. The adsorption of gases on plane surfaces of glass, mica and platinum. *J. Am. Chem. Soc.* **1918**, *40*, 1361–1403. [CrossRef]
65. Freundlich, H. Über die adsorption in lösungen. *Z. Phys. Chem.* **1907**, *57*, 385–470. [CrossRef]
66. Temkin, M.I. Adsorption equilibrium and the kinetics of processes on nonhomogeneous surfaces and in the interaction between adsorbed molecules. *Zh. Fiz. Chim.* **1941**, *15*, 296–332.
67. Lagergren, S.K. About the theory of so-called adsorption of soluble substances. *Sven. Vetenskapsakad. Handingarl* **1898**, *24*, 1–39.
68. Ho, Y.; McKay, G. Pseudo-second order model for sorption processes. *Process. Biochem.* **1999**, *34*, 451–465. [CrossRef]
69. Chen, D.; Yu, X.; Song, C.; Pang, X.; Huang, J.; Li, Y. Effect of pyrolysis temperature on the chemical oxidation stability of bamboo biochar. *Bioresour. Technol.* **2016**, *218*, 1303–1306. [CrossRef]
70. Claoston, N.; Samsuri, A.; Husni, M.A.; Amran, M.M. Effects of pyrolysis temperature on the physicochemical properties of empty fruit bunch and rice husk biochars. *Waste Manag. Res.* **2014**, *32*, 331–339. [CrossRef]
71. Hu, X.; Ding, Z.; Zimmerman, A.; Wang, S.; Gao, B. Batch and column sorption of arsenic onto iron-impregnated biochar synthesized through hydrolysis. *Water Res.* **2015**, *68*, 206–216. [CrossRef]
72. Kang, D.; Yu, X.; Ge, M.; Lin, M.; Yang, X.; Jing, Y. Insights into adsorption mechanism for fluoride on cactus-like amorphous alumina oxide microspheres. *Chem. Eng. J.* **2018**, *345*, 252–259. [CrossRef]
73. Wu, H.; Feng, Q.; Yang, H.; Alam, E.; Gao, B.; Gu, D. Modified biochar supported Ag/Fe nanoparticles used for removal of cephalexin in solution: Characterization, kinetics and mechanisms. *Colloids Surfaces A Physicochem. Eng. Asp.* **2017**, *517*, 63–71. [CrossRef]
74. Matos, T.; Schultz, J.; Khan, M.; Zanoelo, E.; Mangrich, A.; Araújo, B.R.; Navickiene, S.; Romao, L. Using Magnetized (Fe_3O_4 / Biochar Nanocomposites) and Activated Biochar as Adsorbents to Remove Two Neuro-Active Pesticides from Waters. *J. Braz. Chem. Soc.* **2017**. [CrossRef]
75. Li, H.-B.; Dong, X.; da Silva, E.B.; de Oliveira, L.M.; Chen, Y.; Ma, L.Q. Mechanisms of metal sorption by biochars: Biochar characteristics and modifications. *Chemosphere* **2017**, *178*, 466–478. [CrossRef] [PubMed]
76. Zhao, J.; Shen, X.-J.; Domene, X.; Alcañiz, J.-M.; Liao, X.; Palet, C. Comparison of biochars derived from different types of feedstock and their potential for heavy metal removal in multiple-metal solutions. *Sci. Rep.* **2019**, *9*, 1–12. [CrossRef] [PubMed]
77. Zhong, L.-B.; Yin, J.; Liu, S.-G.; Liu, Q.; Yang, Y.-S.; Zheng, Y.-M. Facile one-pot synthesis of urchin-like Fe–Mn binary oxide nanoparticles for effective adsorption of Cd(ii) from water. *RSC Adv.* **2016**, *6*, 103438–103445. [CrossRef]
78. Wan, X.; Li, C.; Parikh, S.J. Simultaneous removal of arsenic, cadmium, and lead from soil by iron-modified magnetic biochar. *Environ. Pollut.* **2020**, *261*, 114157. [CrossRef]
79. Din, S.U.; Azeez, A.; Abdin, Z.U.; Haq, S.; Hafeez, M.; Imran, M.; Hussain, S.; Alarfaji, S.S. Investigation on Cadmium Ions Removal from Water by a Nanomagnetite Based Biochar Derived from Eleocharis Dulcis. *J. Inorg. Organomet. Polym. Mater.* **2020**, *31*, 415–425. [CrossRef]
80. Esfandiari, N.; Kashefi, M.; Mirjalili, M.; Afsharnezhad, S. Role of silica mid-layer in thermal and chemical sta-bility of hierarchical Fe_3O_4-SiO_2-TiO_2 nanoparticles for improvement of lead adsorption: Kinetics, thermodynamic and deep XPS investigation. *Mater. Sci. Eng.* **2020**, *262*, 114690. [CrossRef]
81. Wu, H.; Gao, G.; Zhou, X.; Zhang, Y.; Guo, S. Control on the formation of Fe3O4nanoparticles on chemically reduced graphene oxide surfaces. *CrystEngComm* **2012**, *14*, 499–504. [CrossRef]
82. Yang, T.; He, R.; Nie, G.; Wang, W.; Zhang, G.; Hu, Y.; Wu, L. Creation of Hollow Calcite Single Crystals with CQDs: Synthesis, Characterization, and Fast and Efficient Decontamination of Cd(II). *Sci. Rep.* **2018**, *8*, 17603. [CrossRef]
83. Chowdhury, P.; Athapaththu, S.; Elkamel, A.; Ray, A.K. Visible-solar-light-driven photo-reduction and removal of cadmium ion with Eosin Y-sensitized TiO2 in aqueous solution of triethanolamine. *Sep. Purif.Technol.* **2017**, *174*, 109–115. [CrossRef]
84. Zulfiqar, M.; Lee, S.Y.; Mafize, A.A.; Kahar, N.A.M.A.; Johari, K.; Rabat, N.E. Efficient Removal of Pb(II) from Aqueous Solutions by Using Oil Palm Bio-Waste/MWCNTs Reinforced PVA Hydrogel Composites: Kinetic, Isotherm and Thermodynamic Modeling. *Polymers* **2020**, *12*, 430. [CrossRef] [PubMed]
85. Zhou, Q.; Liao, B.; Lin, L.; Qiu, W.; Song, Z. Adsorption of Cu (II) and Cd (II) from aqueous solutions by ferro-manganese binary oxide–biochar composites. *Sci. Total Environ.* **2018**, *615*, 115–122. [CrossRef]
86. Tong, X.-J.; Li, J.-Y.; Yuan, J.; Xu, R.-K. Adsorption of Cu(II) by biochars generated from three crop straws. *Chem. Eng. J.* **2011**, *172*, 828–834. [CrossRef]
87. Rao, K.S.; Anand, S.; Venkateswarlu, P.J.B. Adsorption of cadmium (II) ions from aqueous solution by Tectona grandis LF (teak leaves powder). *BioResources* **2010**, *5*, 438–454.
88. Jefferson, W.A.; Hu, C.; Liu, H.; Qu, J. Reaction of aqueous Cu–Citrate with MnO2 birnessite: Characterization of Mn dissolution, oxidation products and surface interactions. *Chemosphere* **2015**, *119*, 1–7. [CrossRef] [PubMed]
89. Osasona, I.; Aiyedatiwa, K.; Johnson, J.; Faboya, O.L. Activated carbon from spent brewery barley husks for cadmium ion adsorption from aqueous solution. *Indones. J. Chem.* **2018**, *18*, 145–152. [CrossRef]

90. Sulaymon, A.H.; Ebrahim, S.E.; M-Ridha, M.J. Competitive biosorption of Pb (II), Cr (III), and Cd (II) from synthetic wastewater onto heterogeneous anaerobic biomass in single, binary, and ternary batch systems. *Desalin. Water Treat.* **2014**, *52*, 5629–5638. [CrossRef]
91. Usman, A.; Sallam, A.; Zhang, M.; Vithanage, M.; Ahmad, M.; Al-Farraj, A.; Ok, Y.S.; Abduljabbar, A.; Al-Wabel, M. Sorption Process of Date Palm Biochar for Aqueous Cd (II) Removal: Efficiency and Mechanisms. *Water Air Soil Pollut.* **2016**, *227*, 449. [CrossRef]
92. Doi, A.; Khosravi, M.; Ejtemaei, M.; Nguyen, T.A.; Nguyen, A.V. Specificity and affinity of multivalent ions adsorption to kaolinite surface. *Appl. Clay Sci.* **2020**, *190*, 105557. [CrossRef]
93. Yi, Y.; Huang, Z.; Lu, B.; Xian, J.; Tsang, P.E.; Cheng, W.; Fang, J.; Fang, Z. Magnetic biochar for environmental remediation: A review. *Bioresour. Technol.* **2020**, *298*, 122468. [CrossRef] [PubMed]
94. Mohan, D.; Kumar, A.; Sarswat, A.; Franco, M.A.; Pittman, C.U. Cadmium and lead remediation using magnetic oak wood and oak bark fast pyrolysis bio-chars. *Chem. Eng. J.* **2014**, *236*, 513–528. [CrossRef]
95. Ehrampoush, M.H.; Miria, M.; Salmani, M.H.; Mahvi, A.H. Cadmium removal from aqueous solution by green synthesis iron oxide nanoparticles with tangerine peel extract. *J. Environ. Health Sci. Eng.* **2015**, *13*, 1–7. [CrossRef] [PubMed]
96. Yap, M.; Mubarak, N.; Sahu, J.N.; Abdullah, E.C. Microwave induced synthesis of magnetic biochar from agricultural biomass for removal of lead and cadmium from wastewater. *J. Ind. Eng. Chem.* **2017**, *45*, 287–295. [CrossRef]
97. Hussain, N.; Chantrapromma, S.; Suwunwong, T.; Phoungthong, K. Cadmium (II) removal from aqueous solution using magnetic spent coffee ground biochar: Kinetics, isotherm and thermodynamic adsorption. *Mater. Res. Express* **2020**, *7*, 085503. [CrossRef]
98. Liu, M.; Yang, L.; Zhang, L. Functionalization of magnetic hollow porous oval shape $NiFe_2O_4$ as a highly selective sorbent for the simultaneous determination of five heavy metals in real samples. *Talanta* **2016**, *161*, 288–296. [CrossRef] [PubMed]
99. Trakal, L.; Veselská, V.; Šafařík, I.; Vítková, M.; Číhalová, S.; Komárek, M. Lead and cadmium sorption mechanisms on magnetically modified biochars. *Bioresour. Technol.* **2016**, *203*, 318–324. [CrossRef]
100. Son, E.-B.; Poo, K.-M.; Chang, J.-S.; Chae, K.-J. Heavy metal removal from aqueous solutions using engineered magnetic biochars derived from waste marine macro-algal biomass. *Sci. Total. Environ.* **2018**, *615*, 161–168. [CrossRef]
101. Ruthiraan, M.; Abdullah, E.C.; Mubarak, N.; Noraini, M. A promising route of magnetic based materials for removal of cadmium and methylene blue from waste water. *J. Environ. Chem. Eng.* **2017**, *5*, 1447–1455. [CrossRef]
102. Huang, F.; Zhang, L.; Wu, R.-R.; Zhang, S.-M.; Xiao, R.-B. Adsorption Behavior and Relative Distribution of Cd^{2+} Adsorption Mechanisms by the Magnetic and Nonmagnetic Biochars Derived from Chicken Manure. *Int. J. Environ. Res. Public Heal.* **2020**, *17*, 1602. [CrossRef] [PubMed]
103. Li, R.; Liang, W.; Huang, H.; Jiang, S.; Guo, D.; Li, M.; Zhang, Z.; Ali, A.; Wang, J.J. Removal of cadmium(II) cations from an aqueous solution with aminothiourea chitosan strengthened magnetic biochar. *J. Appl. Polym. Sci.* **2018**, *135*. [CrossRef]
104. Buema, G.; Lupu, N.; Chiriac, H.; Herea, D.D.; Favier, L.; Ciobanu, G.; Litu, L.F.; Harja, M. Fly ash magnetic adsorbent for cadmium ion removal from an aqueous solutions. *Spring* **2021**, *185*, 42–50. [CrossRef]